

**SIMULTANEOUS MEASUREMENT OF 3-D  
DISPLACEMENT COMPONENTS CAUSED BY  
CRACK GROWTH USING CIRCULAR GRATINGS  
MOIRÉ FRINGES AND GRAPHICAL ANALYSIS**

**YEN KIN SAM**

**UNIVERSITI SAINS MALAYSIA**

**2012**

## DECLARATION

I hereby declare that the work reported in this thesis is the result of my own investigation. Materials taken from other sources, either published or unpublished, are duly acknowledged by giving explicit references.

Signature: .....

Name of student: .....

Matrix number: .....

Date: .....

**SIMULTANEOUS MEASUREMENT OF 3-D DISPLACEMENT  
COMPONENTS CAUSED BY CRACK GROWTH USING CIRCULAR  
GRATINGS MOIRÉ FRINGES AND GRAPHICAL ANALYSIS**

**by**

**YEN KIN SAM**

**Thesis submitted in fulfillment of the requirements  
for the degree of  
Doctor of Philosophy**

**May 2012**

## ACKNOWLEDGEMENT

First of all, I would like to express my heartfelt gratitude to my supervisor, Professor Dr. Mani Maran Ratnam, for his support and motivation throughout this research work. His guidance and incisive advice have inspired me to generate fruitful approaches in achieving the objectives in this research. Without his effort, I would not be able to proceed and bring this research to a completion.

Besides, I would like to acknowledge the school dean Associate Professor Dr. Zaldi bin Mohd Ripin and Professor Dr. Zainal Alimuddin b. Zainal Alauddin for their support and recommendation in the application for financial support of RLKA so that I could concentrate to my research work without financial worry. I also want to thank Mr. Ashamuddin, Mr. Baharom and other staffs in School of Mechanical Engineering, USM for their help and support in this research.

My gratitude is extended to my beloved parent, brothers and Ms. Lo Kiah Yann who support me all along without hesitation. I treasure dearly their encouragement and moral support throughout these years.

Last but not the least, my sincere thanks and regards to Tan Kok Tat, Chuah Hun Guan, Teoh Yew Heng, Wong Chee Khoo, Ko Ying Hou, Wong Wai Chee, Chong Chong Liang, Low Jian Haur, Ooi Lu Ean, Lim Kar Loon, Tan Wei Hong and all my ex-course mates and friends, for their unlimited encourage and support.

## TABLES OF CONTENTS

<b>ACKNOWLEDGEMENT</b>	ii
<b>TABLE OF CONTENTS</b>	iii
<b>LIST OF TABLES</b>	vi
<b>LIST OF FIGURES</b>	vii
<b>LIST OF ABBREVIATIONS</b>	xiii
<b>ABSTRAK</b>	xiv
<b>ABSTRACT</b>	xv
<b>CHAPTER 1 - INTRODUCTION</b>	
1.1 Research background	1
1.2 Problem statement	6
1.3 Research objectives	8
1.4 Thesis outline	9
<b>CHAPTER 2 - LITERATURE REVIEW</b>	
2.1 Introduction	11
2.2 Overview of the measurement and monitoring methods for surface cracks	11
2.3 Classification of the various crack measurement methods	12
2.3.1 Linear variable differential transformer (LVDT)	13
2.3.2 Strain gauge and C-shape spring	16
2.3.3 Circuit continuity of Radio Frequency Identification (RFID) tag and conductive materials	18
2.3.4 Electrical resistivity methods	20
2.3.5 Fiber optic sensor (FOS)	22
2.3.6 Photogrammetrics and image analysis methods	26
2.3.7 Potential of the moiré methods in crack measurement and monitoring	28
2.3.8 Commercial devices for crack measurement and monitoring	33

2.3.9	Acoustic methods	38
2.3.10	Summary of the methods	40
2.4	Chapter summary	45

### **CHAPTER 3 - METHODOLOGY**

3.1	Introduction	46
3.2	Eccentricity and 3-D displacement components	49
3.3	Generation of moiré pattern	51
3.4	Transformation of circular gratings moiré pattern	60
3.5	Experimental setup for moiré pattern acquisition	62
3.6	Moiré pattern analysis using Fourier transformation method	64
3.7	Moiré pattern analysis using graphical analysis method	65
3.7.1	Extraction of the moiré fringe center	68
3.7.2	Complex moiré pattern analysis using graphical analysis method	71
3.7.3	ROI analysis for multiple fringe moiré pattern	80
3.7.4	Representation of the transformed moiré fringe as a sinusoidal pattern	82
3.7.5	Two dimensional (2-D) displacement determination from the fitted sine function	84
3.7.6	Algorithm development for graphical analysis method	90
3.7.7	GUI for graphical analysis method	94
3.8	Sensitivity study for graphical analysis method	100
3.9	Three dimensional (3-D) displacement determination using graphical analysis method	105
3.9.1	Principle of the proposed method for 3-D displacement determination	106
3.9.2	$z$ -displacement determination using the SVD method	112
3.9.3	$z$ -displacement determination using the MVD method	121
3.10	Application of the proposed 3-D displacement measurement method on a crack model	128
3.11	Application of the proposed 3-D displacement measurement method on the real wall crack	134
3.12	Chapter summary	138

## **CHAPTER 4 – RESULTS AND DISCUSSION**

4.1	Introduction	140
4.2	Application of graphical analysis method on different types moiré patterns	140
4.2.1	Application to moiré patterns produced by digitally generated gratings	141
4.2.2	Application to moiré patterns produced by real gratings	144
4.3	Application of graphical analysis method in random moiré patterns	148
4.3.1	Single fringe moiré patterns with random 2-D displacements	148
4.3.2	Multiple fringe moiré patterns with random 2-D displacements	151
4.4	Application of graphical method to 3-D displacement sensing	160
4.4.1	<i>z</i> -displacement determination using the SVD method	161
4.4.2	<i>z</i> -displacement determination using the MVD method	164
4.4.3	Discussion and comparison of SVD and MVD methods	168
4.5	Real application of the proposed 3-D displacement determination method in crack growth monitoring	172
4.5.1	Application on the crack model	172
4.5.2	Application to the real wall crack	183
4.6	Chapter summary	196

## **CHAPTER 5 - CONCLUSIONS AND FUTURE WORK**

5.1	Conclusion	198
5.2	Recommendation for future work	199

## **REFERENCES**

### **APPENDICES**

Appendix A	Algorithm development and testing for Fourier transformation method	212
Appendix B	The moiré patterns captured for the real crack growth monitoring.	230
Appendix C	The detailed 3-D displacement components obtained for real crack monitoring.	234

## **LIST OF PUBLICATIONS**

## LIST OF TABLES

		Page
Table 2.1	Summary of the methods / devices and measurement capability	41
Table 3.1	The summarized specifications for the gratings pairs	101
Table 3.2	The summary of data extracted from the fitted curves.	117
Table 3.3	Results of analysis of 3-D displaced moiré patterns and the absolute difference in $A$ .	122
Table 3.4	The detailed data for z-displacement calibration (MVD).	125
Table 4.1	The data and analysis of moiré pattern with 2-D displacements (Single fringe moiré pattern at $\varepsilon_{in} = 0$ ) using graphical analysis method.	150
Table 4.2	The data and analysis of moiré pattern with 2-D displacements (Multiple fringes moiré pattern at $\varepsilon_{in} = 0$ ) using graphical analysis method.	155
Table 4.3	The data extracted from the moiré patterns with various z-displacements (SVD).	162
Table 4.4	The data and absolute difference values extracted from the moiré patterns with various z-displacements (MVD).	165
Table 4.5	Details input and output data for 3-D crack growth measurement	173
Table 4.6	The measurement errors to the translation stage and the to the crack model.	179
Table 4.7	The 3-D displacement outputs determined from the moiré patterns captured in Spot 4 (control unit).	186



## LIST OF FIGURES

		Page
Figure 1.1	The three crack modes (a) opening mode (mode I) (b) sliding mode (mode II) (c) tearing mode (mode III) (The directions of the stresses are indicated by the arrows).	3
Figure 2.1	Mounted LVDT on a concrete specimen. (Source: Picandet et al., 2009)	14
Figure 2.2	Attached strain gauge on a C-shape spring as crack monitoring device. (Source: Johnson and Robertson, 2007)	17
Figure 2.3	Outline of the crack detection system using RFID tag and electrical conductive materials (Source: Morita and Noguchi, 2006)	19
Figure 2.4	Equipments for electrical resistivity measurement on concrete structures. (Source: Lataste et al., 2003)	21
Figure 2.5	(a) Mixed mode crack sensor with two optical fibers at opposite angles and (b) the expected deformation of the optical fiber across crack under mixed mode crack opening. (Source: Wan and Leung, 2007b)	24
Figure 2.6	Attached gratings (Source: Chan et al., 2008)	31
Figure 2.7	Various gauges for crack width measurement (a) Crack Width Ruler (Source: Elcometer®) (b) Crack Width Gauge (Source: Avongard©) (c) Crack comparator (Source: ACI 224.1R-93)	34
Figure 2.8	Commercial devices for crack width monitoring and measurement (a) Crack monitoring sensor (Source: Advanced Optics Solution GmbH) (b) Force Concrete Crack Monitor (Source: FORCE Technology) (c) Fissuro Logger sensor® (Source: SITES©)	36
Figure 2.9	Tell-Tales product series of crack monitoring and measurement (a) Tell-Tale crack meter (b) Avongard Displacement Tell-Tales (c) Crack Progress Chart (Source: Avongard©)	37
Figure 3.1	Theoretical framework for 3-D displacement determination using circular grating moiré pattern	48
Figure 3.2	(a) Eccentricity magnitude $\varepsilon$ and eccentricity direction $\varphi$ of superimposed circular gratings in the $x$ - $y$ plane (b) the $z$ -displacement and the reference axes in 3-D.	50

Figure 3.3	Moiré patterns generated mathematically with different eccentricities $\varepsilon$ .	54
Figure 3.4	Moiré patterns generated by overlapping high-frequency digitally generated gratings with different eccentricities $\varepsilon$ .	55
Figure 3.5	Moiré patterns generated by overlapping low-frequency digitally generated gratings with different eccentricities $\varepsilon$ .	56
Figure 3.6	Moiré patterns generated by overlapping real gratings (single fringe at $\varepsilon = 0$ mm).	58
Figure 3.7	Moiré patterns generated by overlapping commercially available real gratings.	59
Figure 3.8	The spatial transformation of moiré pattern (a) Original circular moiré pattern and (b) transformed rectangular moiré pattern.	61
Figure 3.9	Experimental setup for moiré pattern acquisition.	63
Figure 3.10	The moiré patterns ( $\varphi = 90^\circ$ ) and its transformed version with different $\varepsilon$	66
Figure 3.11	The moiré patterns ( $\varepsilon = 0.300$ mm) and its transformed version with different $\varphi$ .	67
Figure 3.12	(a) Transformed moiré pattern (b) moiré pattern after background normalization (c) detection of the lowest intensity pixels in radial direction as moiré fringe. (d) the extracted coordinates of the fringe center in the polar coordinates.	69
Figure 3.13	Selection of the structuring element and transformed moiré pattern.	70
Figure 3.14	Moiré patterns generated using digitally generated low frequency gratings pair with different eccentricity magnitude $\varepsilon$ and fixed eccentricity direction $\varphi$ at $180^\circ$ .	72
Figure 3.15	Comparison of moiré patterns generated by gratings-pair of 50 and 25 concentric circles.	73
Figure 3.16	(a) Transformed moiré pattern (b) moiré pattern after background normalization (c) detection of the lowest intensity pixels in radial direction as moiré fringe. (d) The extracted coordinates and the unwrapped coordinates of the fringe center in the polar coordinates.	79
Figure 3.17	The division of the fringe pitches within a moiré pattern generated using commercially available gratings (a) original	81

	moiré pattern (b) transformed moiré pattern.	
Figure 3.18	(a) The extracted fringe centers with different eccentricity magnitudes $\varepsilon$ and fixed eccentricity direction $\varphi$ at $90^\circ$ (b) The extracted fringe centers with different eccentricity directions $\varphi$ and fixed eccentricity magnitude $\varepsilon$ at 1.00 mm.	83
Figure 3.19	(a) The plot of output ( $A$ ) against input eccentricity magnitude ( $\varepsilon_{in}$ ) for mathematical generated gratings moiré patterns using graphical analysis method (b) the plot of the output phase shift ( $P$ ) for various input eccentricity magnitudes ( $\varepsilon_{in}$ ) for input eccentricity direction of $\varphi_{in}$ at $90^\circ$ .	87
Figure 3.20	(a) The plot of output ( $\varepsilon_{out}$ ) against input eccentricity magnitude ( $\varepsilon_{in}$ ) for mathematical generated gratings moiré patterns using graphical analysis method (b) the plot of the output phase shift ( $\varphi_{out}$ ) for various input eccentricity magnitudes ( $\varepsilon_{in}$ ) for input eccentricity direction of $\varphi_{in}$ at $90^\circ$ .	88
Figure 3.21	Output of various stages of the graphical analysis method using a moiré pattern generated by commercially available gratings as input image.	92
Figure 3.22	Flowchart of the graphical analysis method.	93
Figure 3.23	The interface of the developed GUI.	94
Figure 3.24	(a) The popup windows for image file browsing and selecting saved in the computer. (b) The loaded image in the GUI containing the moiré pattern for analysis.	96
Figure 3.25	(a) The cropped region in the enlarged grayscale moiré pattern. (b) The reloaded moiré pattern in the image display pan after the cropping operation.	98
Figure 3.26	(a) The triggered GUI for 2-D displacement determination from the cropped moiré pattern. (b) The results of the 2-D displacement determination displayed in the results panel.	99
Figure 3.27	Moiré pattern in zero relative displacement created by the (a) gratings-pairs 1, (b) gratings-pairs 2, (c) gratings-pairs 3 and (d) gratings-pairs 4 and (e) – (h) are the corresponding moiré patterns with $\varepsilon = 1.00$ mm and $\varphi = 180^\circ$ .	102
Figure 3.28	(a) Amplitude $A$ versus input eccentricity magnitude $\varepsilon_{in}$ for different gratings ratios. (b) Phase shift $P$ versus input eccentricity magnitude $\varepsilon_{in}$ for different gratings ratios orientated at $90^\circ$ .	103
Figure 3.29	Sensitivity of the moiré pattern versus grating ratio.	104

Figure 3.30	The viewing directions relative to the grating plane.	107
Figure 3.31	Moiré pattern sets with different 3-D displacements from various viewing directions.	108
Figure 3.32	(a) Moiré patterns formed by various 3-D displacement inputs (b) transformed moiré patterns by various 3-D displacement inputs.	109
Figure 3.33	Relationship between the formation of moiré patterns and the $z$ -displacement due to different viewing directions.	111
Figure 3.34	The fitted curves of the fringe centers for the transformed moiré fringes.	114
Figure 3.35	(a) The input (mm) versus the output (mm) of eccentricity magnitudes. (b) The comparison of the input ( $^{\circ}$ ) and output ( $^{\circ}$ ) eccentricity directions.	118
Figure 3.36	Offset $C$ versus $z_{in}$ (mm) for different $\varepsilon_{in}$ .	119
Figure 3.37	Compensated offset $C$ versus $z_{in}$ (mm) for different $\varepsilon_{in}$ .	120
Figure 3.38	$z_{in}$ (mm) versus $z_{out}$ (mm) after calibration.	120
Figure 3.39	The relationship between the absolute difference in 2-D displacement and $z$ -displacements.	124
Figure 3.40	The calibration plots for MVD methods to obtain outputs $z$ -displacements.	127
Figure 3.41	The crack model.	129
Figure 3.42	The setup for the demonstration of using developed method for crack growth measurement on crack model.	130
Figure 3.43	The starting moiré pattern at zero crack growth.	132
Figure 3.44	The moiré patterns captured due to the 3-D crack growth.	133
Figure 3.45	The attachment of the gratings sets for wall crack monitoring.	135
Figure 3.46	The setup for moiré pattern capturing using a tripod for camera positioning.	137
Figure 3.47	Moiré patterns captured at Spot 1, Spot 2, Spot 3 as well as Spot 4 throughout the monitoring period.	138
Figure 4.1	(a) Plot of output ( $\varepsilon_{out}$ ) against input eccentricity magnitude ( $\varepsilon_{in}$ ) for high frequency gratings moiré patterns using	142

	graphical analysis method (b) plot of the output eccentricity direction $\varphi_{out}$ for various input eccentricity magnitudes for input eccentricity direction of $\varphi_{in}$ at $90^\circ$ .	
Figure 4.2	(a) Plot of output ( $\varepsilon_{out}$ ) against input eccentricity magnitude ( $\varepsilon_{in}$ ) for low frequency gratings moiré patterns using graphical analysis method (b) plot of the output eccentricity direction $\varphi_{out}$ for various input eccentricity magnitudes for input eccentricity direction of $\varphi_{in}$ at $90^\circ$ .	143
Figure 4.3	(a) Plot of averaged amplitude $A$ against different input eccentricity magnitudes. (b) The calibrated outputs $\varepsilon_{out}$ versus the inputs $\varepsilon_{in}$ .	145
Figure 4.4	The average outputs $\varphi_{out}$ determined from various input moiré patterns (fixed eccentricity directions of $90^\circ$ ).	146
Figure 4.5	The average outputs $\varphi_{out}$ determined from various inputs $\varphi_{in}$ moiré patterns.	147
Figure 4.6	Moiré patterns with various eccentricity magnitudes $\varepsilon_{in}$ and directions $\varphi_{in}$ .	149
Figure 4.7	(a) Plot of amplitudes, $A$ against different input eccentricity magnitudes using calibration data. (b) The calibrated outputs $\varepsilon_{out}$ versus the inputs $\varepsilon_{in}$ .	152
Figure 4.8	The outputs $\varphi_{out}$ determined from the input moiré patterns (fixed eccentricity directions of $90^\circ$ ).	153
Figure 4.9	Moiré patterns with various eccentricity magnitudes $\varepsilon_{in}$ and directions $\varphi_{in}$ .	154
Figure 4.10	(a) The outputs $\varepsilon_{out}$ determined from various inputs $\varepsilon_{in}$ moiré patterns (b) the error analysis for the outputs $\varepsilon_{out}$ determination using improved graphical method.	158
Figure 4.11	The outputs $\varphi_{out}$ determined from various inputs $\varphi_{in}$ moiré patterns (b) the error analysis for the outputs $\varphi_{out}$ determination using improved graphical method.	159
Figure 4.12	2-D displacement determination from the captured moiré patterns in the presence of $z$ -displacements.	161
Figure 4.13	The outputs versus the inputs $z$ -displacement of moiré patterns determined from the single (normal) viewing direction.	163
Figure 4.14	The error distribution of the determined $z$ -displacement outputs.	164

Figure 4.15	The outputs versus the inputs $z$ -displacement of moiré patterns determined from the MVD.	167
Figure 4.16	The error distribution of the determined $z$ -displacement outputs from MVD method.	167
Figure 4.17	(a)-(c) The determined 3-D components for $x$ -, $y$ - and $z$ -displacement from the captured moiré patterns due to 3-D crack growth.	175
Figure 4.18	(a)-(c) The output errors of the determined 3-D components for $x$ -, $y$ - and $z$ -displacement using the developed graphical analysis method.	176
Figure 4.19	The arrangement of the gratings pairs without the knowledge of the direction for $z$ -displacement.	181
Figure 4.20	The crack growth conditions in $z$ -displacement and the possible collision with gratings plate. (a) without the $z$ -displacement growth (b) $z$ -displacement growth without collision to the gratings plate (c) $z$ -displacement growth collides with the gratings plate.	182
Figure 4.21	The 3-D displacement components change monitored at Spot 4. (a) The $x$ -displacement changes during the monitoring period. (b) The $y$ -displacement changes during the monitoring period. (c) The $z$ -displacement changes during the monitoring period.	184
Figure 4.22	The 3-D displacement components change monitored at Spot 1. (a) The $x$ -displacement changes during the monitoring period. (b) The $y$ -displacement changes during the monitoring period. (c) The $z$ -displacement changes during the monitoring period.	188
Figure 4.23	The 3-D displacement components change monitored at Spot 2. (a) The $x$ -displacement changes during the monitoring period. (b) The $y$ -displacement changes during the monitoring period. (c) The $z$ -displacement changes during the monitoring period.	190
Figure 4.24	The 3-D displacement components change monitored at Spot 3. (a) The $x$ -displacement changes during the monitoring period. (b) The $y$ -displacement changes during the monitoring period. (c) The $z$ -displacement changes during the monitoring period.	192
Figure 4.25	The gratings attached to at Spot 1.	194

## LIST OF ABBREVIATION

		Page
SHM	Structural health monitoring	2
ACI	American Concrete Institute	3
LVDT	Linear Variable Differential Transformer	3
FOS	Fiber Optic Sensor	3
RFID	Radio Frequency Identification	18
FBG	Fiber Bragg Grating	23
ROI	Region of Interest	27
N.I.S.T	National Institute of Standards and Technology	63
$R^2$	Coefficient of Determination	86
SVD	Single viewing direction	112
MVD	Multiple viewing directions	112

**PENGUKURAN KOMPONEN-KOMPONEN SESARAN 3-D SECARA  
SERENTAK YANG DISEBABKAN OLEH PENGEMBANGAN RETAKAN  
DENGAN PINGGIR MOIRÉ JERJI BULATAN DAN ANALISIS GRAFIK**

**ABSTRAK**

Retakan dikenalpasti sebagai punca utama dalam kegagalan sesuatu struktur konkrit. Dengan memantau pertumbuhan retakan, tindakan awal boleh diambil untuk memulihkan struktur konkrit daripada kegagalan. Untuk mengesan ketiga-tiga mod retakan iaitu, mod membuka, mod gelongsor dan mod mengoyak, kaedah yang boleh mengukur ketiga-tiga komponen sesaran 3-D secara serentak dengan penetapan tunggal diperlukan. Corak moiré yang terbentuk dengan pertindihan dua jeriji bulatan dengan pic-picnya yang sedikit berbeza dicadangkan sebagai alat pengukuran kerana corak moiré boleh diulangi dan unik bagi sesuatu sesaran sesatah (2-D) antara kedua-dua jeriji tersebut. Sifat-sifat gelombang, iaitu amplitud dan peralihan fasa yang diekstrak dari corak moiré yang telah ditransformasikan dalam satah polar adalah berpadanan kepada magnitud dan arah kesipian kedua-dua jeriji itu. Dengan ini, kaedah analisis grafik dibangunkan untuk memperoleh maklumat sesaran sesatah (2-D) daripada corak moiré jeriji bulat itu. Dengan wujudnya jurang di antara satah-satah jeriji bulatan ini, corak moiré yang berbeza dapat diperhatikan dari arah normal dan arah bersudut dengan satah jeriji. Perbezaan mutlak sesaran sesatah (2-D) yang diwakili oleh dua corak moiré yang dirakam dari arah-arrah yang berbeza adalah dikaitkan dengan sesaran luar satah bagi kedua-dua jeriji. Berdasarkan kaedah analisis grafik, satu kaedah pengukuran sesaran luar satah dibangunkan untuk menentukan komponen-komponen sesaran 3-D secara serentak.



**SIMULTANEOUS MEASUREMENT OF 3-D DISPLACEMENT  
COMPONENTS CAUSED BY CRACK GROWTH USING CIRCULAR  
GRATINGS MOIRÉ FRINGES AND GRAPHICAL ANALYSIS**

**ABSTRACT**

Cracking is well-known to be a major cause of failures in concrete structures. By monitoring the growth of cracks, early remedial measure can be taken to save the structure from failure. To sense all the three crack modes namely, opening mode, sliding mode and tearing mode, a method that is able to measure the 3-D displacement components simultaneously with a single setting is needed. The moiré pattern formed by overlapping two circular gratings with slightly different pitches is proposed as a measurement tool because the moiré pattern is repeatable and unique for a relative in-plane (2-D) displacement between the two gratings. The wave properties, i.e. the amplitude and phase shift extracted from the transformed moiré fringe in the polar plane directly corresponds to the eccentricity magnitude and direction of the two gratings. Thus, graphical analysis method is developed to extract the 2-D displacement information from the circular gratings moiré pattern. In the presence of a gap between the two grating planes, different moiré patterns can be observed from the normal and off-normal viewing directions with the grating plane. The absolute difference of the 2-D displacement represented by the two moiré patterns captured from different viewing directions is related to the out-of-plane displacement between the two gratings. Based on the developed graphical analysis method, an out-of-plane displacement measurement method is established for the simultaneous 3-D displacement components determination.

# CHAPTER 1

## INTRODUCTION

### 1.1 Research background

Concrete structures are subjected to various factors that contribute to cracking. These include static and dynamic stresses due to permanent and working loads, repeated expansion and contraction due to weather and ambient temperature changes (thermal stress), intrusion of moisture (frost-deicing stress), nearby vibration effects, soil movement and impact loading. The cracks may further grow and lead to an extremely hazardous situation that may finally result in the failure of the structure.

Cracking is especially critical for large concrete structures, such as dams, bridges, edifices, highway etc., because a great amount of concrete has been set to become a structural body during construction. Once crack occurs on the surface, the highly repetitive working loads, such as vehicle loading on a bridge, or permanent loads such as the water pressure on the dam walls would introduce concentrated stress on the crack area. These phenomena lead to the expansion of the crack width and propagation of the cracks to the whole body of concrete structure. The expansion and growth of the cracks due to continuous loading and other stresses result in failure of the structures. Furthermore, cracks permit the intrusion of moisture and the corrosive chemicals that would further weaken the concrete structures by causing corrosion in the reinforcing steel bars, thus, exposing the concrete structures to catastrophic failure. As safety and reliability become major concerns, tight monitoring and control of the cracks are needed so that remedial actions and

reinforcement can be provided to save and extend the durability and serviceability of the concrete structures.

Crack is a common defect and a sign of deterioration of the concrete structures that appears once the placement of the concrete is done (Chang et al., 2003). Surface cracks on a concrete structure are visible and therefore measurable. Besides degrading the aesthetic appearance of the structure, cracks could indicate a major problem that needs urgent attention (Zhu et al., 2011). As it is directly related to the physical health of the concrete structures, cracks are monitored to determine the extent of the deterioration of the structures. The crack pattern, the density of the cracks, the rate of the crack expansion as well as the direction of crack propagation provide a lot of information to engineers and building surveyors for structural health monitoring (SHM). By monitoring the growth of cracks early remedial measure can be taken to save the cracks in concrete.

Generally, crack growth or propagation can be categorized into three modes according to the types and directions of the stresses acting on the crack plane as shown in Figure 1.1. The three crack modes are mode I crack (opening mode) caused by a tensile stress normal to the plane of the crack resulting a pure expansion of the crack, while mode II crack (sliding mode) caused by a shear stress acting parallel to the plane of the crack and perpendicular to the crack front causing an in-plane displacement growth between the two sides of the crack. The mode III crack (tearing mode) caused by a shear stress acting parallel to the plane of the crack and parallel to the crack front leading to an out-of-plane displacement growth between the two sides the crack. The main requirement for a method to sense all three modes of crack

growth simultaneously is the ability to measure the 3-D displacement. However, to date, a method for measuring all three components of displacement simultaneously in a concrete structure has not been reported.

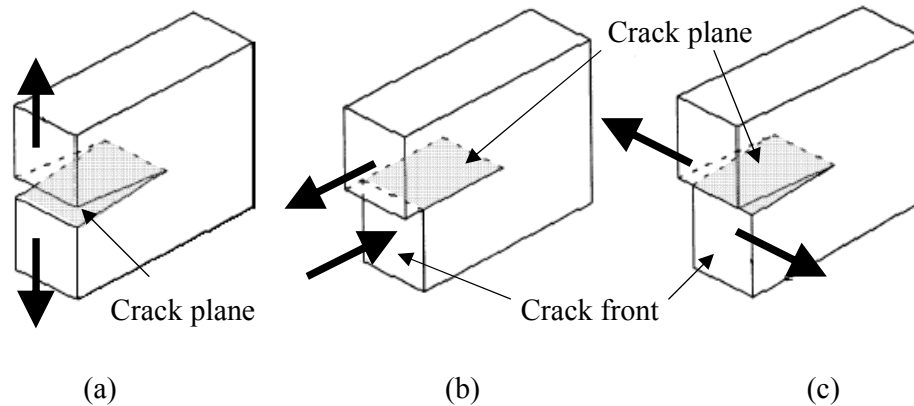


Figure 1.1: The three crack modes (a) opening mode (mode I) (b) sliding mode (mode II) (c) tearing mode (mode III) (The directions of the stresses are indicated by the arrows).

Crack growth monitoring is one of the structural health monitoring activities that is performed regularly to ensure that the concrete structures are in good condition in terms of safety, reliability as well as its functionality. To date, there are numerous methods used for crack growth monitoring on concrete structures. These methods include the direct measurement of the crack width using rulers and digital calipers as well as commercially available devices such as the Crack Width Ruler and Tell-Tale, suggested by American Concrete Institute (ACI) Committee 224 (ACI 224.1R-93). With the advancement of science and technology, many other crack monitoring methods have been developed by combining different areas of study such as the application of linear variable differential transformer (LVDT), fiber optics sensor (FOS), strain gauge, electrical resistivity gages and photogrammetry.

However, the existing methods have various limitations such as limited sensitivity and resolution (e.g. rulers and calipers), need for human involvement in the measurement readouts (e.g. Crack Width Ruler and Tell-Tale products) and limited directionality i.e. 1-D or 2-D measurement only (e.g. FOS, LVDT and photogrammetry).

Circular gratings moiré fringes was shown to have significant potential for 2-D displacement measurement in crack growth monitoring by matching the captured moiré patterns to the reference patterns (Chen et al. (2008) and Yen and Ratnam (2010)). The moiré pattern was formed by two overlapped circular gratings each printed on transparent and white acrylic plates and attached to both sides of the crack. The moiré method enabled the detection and measurement of both  $x$ - and  $y$ -displacements (mode I and II cracks) caused by crack growth with a sensitivity of 0.02 mm (Yen and Ratnam, 2010). The moiré method using circular gratings, in fact, has potential to be extended to the measurement of all the 3-D displacement components. When there is a gap between the planes of the overlapping gratings, the circular gratings pair produces different moiré patterns when viewed from different angles relative to the normal of the grating plane. The change in the moiré pattern depends directly on the gap width between the grating planes and the viewing directions. The gap width is, indeed, the out-of-plane displacement between the two overlapping circular gratings. Thus, the moiré pattern is not only sensitive to in-plane displacement but also sensitive to out-of-plane displacement between the two gratings.

In previous work (Chen et al. (2008) and Yen and Ratnam (2010)), a huge storage of reference images is needed for pattern matching to achieve a fine resolution in the measurement. This not only requires a large memory space for storage of reference images but also is time consuming for both preparing the reference images and patterns matching for displacement determination. To counter this limitation, a method to determine the 2-D in-plane displacement information directly from the moiré pattern is needed. The moiré method, in fact has the potential to be further improved in aspect of the resolution and the sensitivity compared to the previous published works (Chen et al. (2008) and Yen and Ratnam (2010)). However, to date, no previous study has been carried out for the 2-D displacement determination using image analysis algorithm to analyze the circular gratings moiré pattern.

A detailed study is needed to extend the application of the moiré method for a complete crack growth displacement sensing and measurement in 3-D. To measure the 3-D displacement components, the proposed method must have the ability to determine the 2-D displacement components (eccentricity magnitude and direction or the in-plane  $x$ - and  $y$ -displacements) between the two overlapped gratings from the moiré pattern. For the out-of-plane displacement determination (or the  $z$ -displacement), the absolute displacement between the moiré patterns observed in normal and off-normal viewing directions is analyzed using the proposed method and relate it to the gap width between the two circular gratings. Thus, in this work, the 3-D displacement components measurement by analyzing the circular gratings moiré patterns is proposed to sense and measure all the three modes crack growth simultaneously.

In the following sections, the main problems of the proposed moiré method for in-plane (2-D) and out-of-plane displacement (3-D) for crack growth monitoring and measurement are addressed. The research objectives and the approach are defined before the presentation of the thesis outline at the end of the chapter.

## **1.2 Problem statement**

To sense and measure all the three modes (i.e., opening, sliding and tearing crack modes) of crack growth on a concrete structure simultaneously, a 3-D displacement measurement method is needed. Although the moiré method has shown its potential for simultaneous 3-D displacement measurement, there is no study and research reported to date in any published literature.

In the previous work (Chan et al. (2008) and Yen and Ratnam (2010)), pattern matching was proposed to extract the displacement information by comparing the captured image to the stored reference images. The resolution of the method is limited to the step displacement of the stored reference images in database. The step displacement refers to a constant displacement value used to generate a set of reference moiré patterns within a desired measurement range. For example, a measurement range of 0 mm to 3 mm with a step of 0.002 mm needs a total of 1501 reference moiré patterns, otherwise the measured displacement outputs could be in error. To increase the resolution of the measurement, a huge database of the reference images covering all possible moiré patterns generated for different displacements is needed. Pattern matching with a huge storage is not only a time consuming process but also a waste of a computer memory space. Besides, in the

pattern matching method, the displacement value is determined from the best match reference pattern. There is no interpolation between the step reference patterns. Error tends to occur if the input moiré pattern was generated with the intermediate value within a step displacement. This method is thus clearly not suitable for very fine and sensitive measurement.

To reduce the dependency on a large database of reference images and to enable high sensitive measurement, a direct interpretation of the moiré pattern for the 2-D displacement determination is desired. The moiré patterns formed by two overlapped circular gratings with slightly different pitches are uniquely sensitive to a minute change in the planar displacement in terms of eccentricity magnitude and direction. However, the direct interpretation of circular gratings moiré pattern graphically to determine the 2-D displacement information (eccentricity magnitude and direction) is not reported to date.

Park and Kim (1994) proposed a mathematical method to analyze the circular gratings moiré pattern for the 2-D displacement determination. However, this method is based on the assumption that the transmittance of the gratings is sinusoidal and can be expressed in harmonic terms. In the real world, only high frequency gratings, e.g. gratings with 6  $\mu\text{m}$  and 24  $\mu\text{m}$  pitches have sinusoidal-like transmittance. For the application in wall crack monitoring, low frequency gratings with grating pitches larger than 0.50 mm each are used. Thus, a detail study of Park and Kim's method for the application on low frequency circular gratings is necessary.



As mentioned in the previous section, when a gap is present between the two overlapped gratings, the moiré pattern appears differently when viewed from different viewing directions. This effect has been used by previous researcher to detect the in-plane rotation angle of a head-mounted display (Lay and Chen, 1998). But, the possibility of 3-D displacement measurement has not been explored.

### **1.3 Research objectives**

The objectives of this research are as follows:

1. To develop a novel graphical analysis method for in-plane (2-D) displacement components determination directly from the circular gratings moiré pattern and compared its effectiveness and applicability to Fourier transformation method proposed by Park and Kim (1994).
2. To develop a new approach of simultaneous 3-D displacement components determination by analyzing the circular gratings moiré patterns captured in single and multiple viewing directions.
3. To examine the applicability and practicality of the developed method of simultaneous 3-D displacement components determination in the application of cracks growth monitoring on a crack model and the concrete wall.

## 1.4 Thesis outline

The thesis is arranged as follows. The crack measurement methods in the published literatures as well as the commercially available methods are reviewed in Chapter 2. The advantages and the limitations of the existing techniques for crack growth measurement are discussed in detail.

The 2-D and 3-D displacement measurement methods are proposed in Chapter 3. The findings from the previously published method (Park and Kim, 1994) for analyzing the circular gratings moiré pattern for the 2-D displacement determination are briefed in this chapter. Detailed discussion of Park and Kim (1994)'s method are presented in Appendix A. A simpler and novel graphical analysis method to derive the 2-D displacement information directly from the moiré pattern is then proposed. Detailed algorithm of the graphical analysis method is described in this chapter. Besides, the relationship between the gap width between the two overlapped gratings and the moiré patterns viewed from different viewing directions is also discussed in Chapter 3. The difference of the viewed moiré patterns from different viewing directions is quantified and related to the gap width for the out-of-plane displacement determination.

The demonstration of the developed method for 3-D displacement components measurement for crack growth monitoring is presented in Chapter 3. A crack model was designed to simulate the crack growth in 3-D. The developed method determines the 3-D outputs ( $x$ -,  $y$ - and  $z$ -displacement) and compared to values measured using digital dial gages mounted in  $x$ -,  $y$ -, and  $z$ -axis. The

demonstration is also extended to monitor the real cracks on a concrete wall. The outcomes from the two demonstrations are vital parameters to figure out the applicability and practicality of the developed method.

The results and discussions of the experiments and demonstrations are presented in Chapter 4. The proposed graphical analysis method are compared to Park and Kim (1994)'s method based on the obtained outputs and error analysis. A better method for 2-D displacement information determination is drawn to analyze the moiré patterns viewed from different directions for 3-D displacement determination. The results and discussions for the experiment using the proposed 3-D displacement components measurement are also presented in this chapter. Subsequently, the outcomes of the demonstrations using the developed method to measure the crack growth on a crack model and on a concrete wall are discussed in this chapter.

Finally, the conclusions of the research are drawn in Chapter 5. Recommendation and suggestions are given for the future work.

## **CHAPTER 2**

### **LITERATURE REVIEW**

#### **2.1 Introduction**

Various methodologies and practices that have been researched upon and developed in the past to measure and monitor the growth of cracks on concrete structures are reviewed in this chapter. The advantages and the disadvantages of each method are discussed. The present and future trends of the crack monitoring methods are also presented. The methods are classified into its technological basis, namely linear variable differential transformer (LVDT), fiber optic sensor (FOS), acoustics or ultrasonic, photogrammetric methods, electrical resistivity and moiré methods. Commercial devices are also included in the discussion in order to provide a complete review. A special attention will be given to recently published research works related to the measurement and monitoring methods for surface cracks.

#### **2.2 Overview of the measurement and monitoring methods for surface cracks**

Direct measurement of the width of the crack on concrete structures using rulers and simple gauges is the most common and conventional method for crack monitoring. However, these methods have low sensitivity and accuracy for close monitoring and measurement. American Concrete Institute (ACI) Committee 224 (ACI 224.1R-93) has identified several evaluation methods for cracks on concrete structures. These methods include direct and indirect measurement using crack comparator (developed by Edmond Scientific Co. Ltd.), crack monitor (developed by

Avongard Ltd.) and LVDT as well as nondestructive testing (NDT) for internal cracks, voids and the depth of penetration of cracks visible at the surface. The recommended NDT methods are the use of through-transmission technique (ASTM C597) and radiography (using x-ray and gamma-ray).

Alongside with the evolution of the technology, many other highly sensitive and accurate crack monitoring and measurement methods have been developed in the past, such as the fiber optics sensor (FOS) method and photogrammetric method. Although research and development of various crack monitoring methods have started several decades since 1960s the various crack monitoring methods available in the literature have not been reviewed and published before. This chapter aims at presenting and discussing the various methodologies and practices that had been developed and adopted by researchers in the past to measure and monitor cracks and their growth. The advantages and disadvantages of each method are discussed.

### **2.3 Classification of the various crack measurement methods**

Various techniques and equipments from different principles and fields of study were researched and developed in the past for the purpose of crack monitoring and measurement. These methods include the application of LVDT, FOS, acoustics and ultrasonic methods, photogrammetric methods, electrical resistivity and moiré methods. In this chapter, the reviewed methods are classified based on the science and technological principles in different fields of study. The devices that are currently available in the market are also discussed in an independent section in order to provide a more thorough review.

### **2.3.1 Linear variable differential transformer (LVDT)**

The application of Linear Variable Different Transformer (LVDT) is the most common technique in not only crack measurement but also in various measurement applications involving linear displacement. An LVDT has three coils wound around a cylindrical tube. AC current is supplied to the primary coil, inducing voltages on the other two secondary coils which are connected in anti-series. As the LVDT core (e.g. a metal ferromagnetic rod) displaces off centre inside the tube, a difference in voltage occurs between the two induces voltages in secondary coils. The core displacement can thus be determined by measuring the differential of the two induced voltages (Schaevitz Engineering, 1982).

LVDT has become an important tool for structural health monitoring as it is able to measure the linear displacement of the cracks width mechanically and produces corresponding electrical signal output. High sensitivity and accuracy up to 0.001 mm make the LVDT a favorite measurement device in several laboratory measurements (Figure 2.1). In the study of the crack effect on the gas and water permeability, Picandet et al. (2009) used the LVDT to monitor the change of the crack width on a concrete within the micron scale. Oh and Kim (2007) and Tammo and Thelandersson (2006) demonstrated the application of the LVDT to measure the crack width in reinforced concrete structures in their studies.

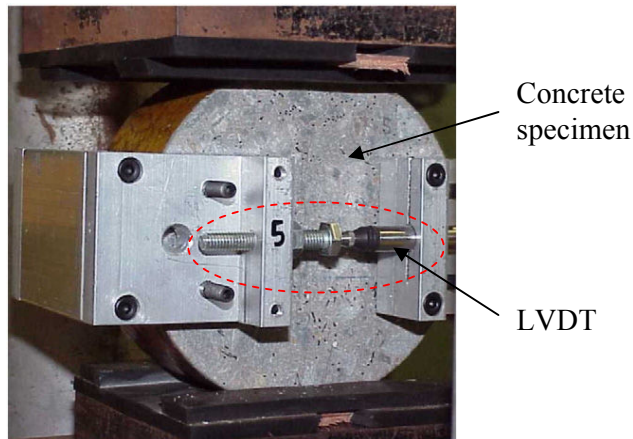


Figure 2.1: Mounted LVDT on a concrete specimen. (Source: Picandet et al., 2009)

The readings of LVDT are always used as benchmark values to compare with other crack measurement methods. Wan and Leung (2007a) and Zhang and Ansari (2005) used the LVDT in the development of FOS methods to measure the width of the crack tip opening. This displacement transducer was also used by Boulay et al. (2009) to study of the relationship between the electrical resistivity of the concrete and the cracking phenomena. In practical application, the LVDT has been attached to the building to measure the concrete cracks, for instance, monitoring the crack width on the Gröndals Bridge in Sweden to predict the tendency of the crack propagation after the reinforcement (Täljsten et al. 2007).

The LVDT is considered to have an infinite resolution as it is operated frictionless with the sliding core and the inductive readout technique. Fine resolution up to  $1\ \mu\text{m}$  is possible for a LVDT in practical application but the resolution could be limited by the noise and resolution of the readout electronics (Trietley, 1986). However, more sophisticated circuitries are needed to achieve the full rated accuracy of LVDT. Usually, this will increase the cost of the equipment, maintenance and require electrical shield or protection in adverse weather condition.

Another concern of using LVDT for structural health monitoring is that the LVDT is susceptible to stray AC magnetic fields. The interference would occur between the generated electromagnetic field and the external electromagnetic or AC magnetic field. The output reading of LVDT can be easily biased by the interferences and thus result in inaccurate data.

Application of LVDT in the monitoring and measurement of the crack widths on concrete structures is a common and conventional method. High sensitivity and accuracy are the reasons for LVDT to become a favorite choice for civil engineers and surveyors. However, the design of the LVDT that only allows the core to slide in one axis limits the LVDT for only 1-D measurement. As the propagation and expansion of the cracks may occur in different angles and unknown orientations, consideration is needed for the installation axis. Multiple LVDT can be used to monitor displacements along more than one axis but this increases cost. For example, three sets of LVDTs can be used to monitor a crack on concrete structure in three axes if the mode of crack is not known. This will increase not only the cost of equipment, but also increase the complexity of the wiring for measurement readouts. As a result, LVDT would be a good option to measure the cracks if the propagation and expansion is predictable, for instance controlled cracks in a laboratory or cracks in a constrained development.



### 2.3.2 Strain gauge and C-shape spring

The wire strain gauge is commonly used to measure strain in deformed materials by means of compressing or tensioning. It converts the applied strain due to the deformation of the attached materials to the electrical resistance. The electronic readout for strain gauge is usually done by integrating it with the Wheatstone bridge. Measurement using strain gauge can be up to very fine scale. The magnitude of the readings is usually expressed in microstrain ( $10^{-6}$ ).

In concrete material study, wire strain gauge is recommended for measuring the deformation of the concrete under compression (ASTM 469-02). A clip gauge had been suggested by Harris and Piersol (2002) to monitor the displacement of its two legs. It was devised by attaching strain gauges on the upper and the lower of the backbone of a C-shape spring. The underlying theory behind is that the strain within the elastic limit, caused by the deflection of the backbone always complies with Hooke's law and the displacement could be calculated using the measured strain value.

A crack gauge device was developed by Johnson and Robertson (2007) for the purpose of concrete crack monitoring and measurement by adopting the idea of the clip gauge (Harris and Piersol, 2002) as shown in Figure 2.2. The developed crack gauge device has the smallest observable crack mouth opening displacement (CMOD) up to 0.00022 inches or 0.005588 mm.

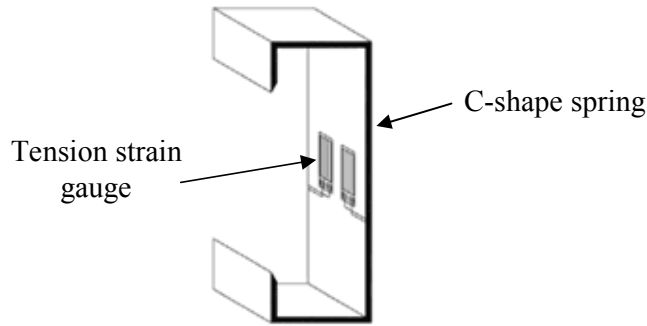


Figure 2.2: Attached strain gauge on a C-shape spring as crack monitoring device.

(Source: Johnson and Robertson, 2007)

Sinclair (2001) suggested that, for very small displacements, the strain gauge can be used instead of LVDT. Strain gauge indeed shows its superior very fine scale measurement with microstrain detection. However, as in LVDT method, the crack monitoring of this method is limited to only 1-D or the mode I crack (opening mode). Multiple gauges should be provided for multiple axes monitoring on mode II and III cracks. A major concern of using strain gauge for structural health monitoring is that the conductive material of the strain gauge is sensitive to the change of temperature. It is because the resistance (conductivity) of the gauge materials could be affected by the temperature and produce inconsistent readings as well as errors. Besides, there are two identified sources of systematic errors that are formed by the effect of temperature change on the strain gauge material itself and the effect of thermal expansion interactions between the gauge and attached material. The methods of the compensation of the temperature effects and the thermal output compensation techniques had been described in the literature (Johnson and Robertson, 2007). Although the thermal effect could be compensated, failing in the representation of the nonlinear temperature effect into a narrow range of linear function and the wrong selection of the coefficients of thermal expansion could produce erroneous outputs.

Johnson and Robertson (2007) commented on the portability of the strain gauge that the gauge should be left installed for long-term measurements without disconnecting and reconnecting the data acquisition system. Otherwise, the initial reading will be lost. In practical use for measuring and monitoring cracks on concrete structures, the long term change of the ambient temperature and weather could be unpredictable and failure in temperature effect compensation would cause critical error in the readings. Perhaps, heat insulation and electrical shield should be provided to eliminate the temperature effects on both the gauge and the readout. Secure wiring and the installation of the strain gauge could also be an important concern to avoid any malfunction caused by heat and weathering effect which could bring moisture to the devices.

### **2.3.3 Circuit continuity of Radio Frequency Identification (RFID) tag and conductive materials**

Morita and Noguchi (2006) have developed a crack detection system based on the electrical circuit theory of continuity. An electrically conductive material (paint or printed coatings with different line widths) was attached across a crack or the part where the crack will occur. This material was connected to a Radio Frequency Identification (RFID) tag to complete the electrical circuit. A transmitter is used to communicate with the RFID tag to estimate the crack width level based on the continuity of the tag circuit. The overall outline of the idea is illustrated in Figure 2.3. Discontinuity of the different line widths of the conductive material indicates the different levels of the crack width. A similar concept was proposed by Pour-Ghaz and Weiss (2011) by using the electrical impedance spectroscopy to detect the time,

location and approximate number of cracks on the surface of concrete. An electrically conductive thin film was applied to the surface of the cementitious materials and the electrical resistance of this film was monitored as the substrate cracks. Although these methods could not be used to quantify the crack width, however, it could be used to indicate the occurrence or expansion of crack and the level of the crack widths.

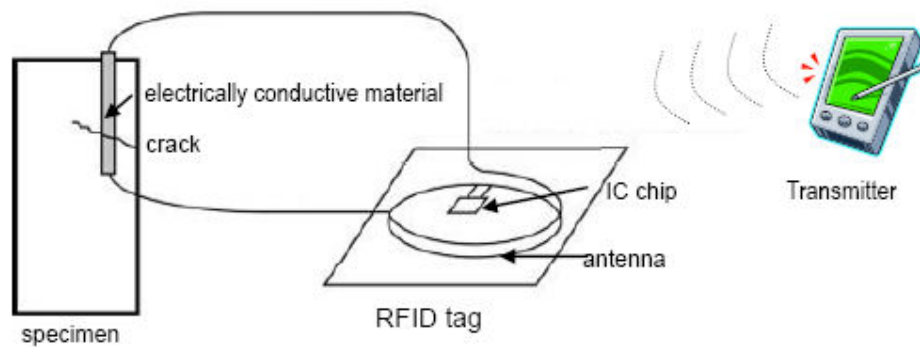


Figure 2.3: Outline of the crack detection system using RFID tag and electrical conductive materials (Source: Morita and Noguchi, 2006)

One of the major advantages of these methods is that the application of the conductive paints or printed coatings or thin film could be done to cover a wide area for multi-cracks monitoring purpose. By using only one transmitter, multiple cracks monitoring is enabled. However, this method could not provide any quantitative reading of the crack growth. Thus, tight monitoring of critical cracks on concrete structures for example, on the dams and bridges, is not possible.

#### 2.3.4 Electrical resistivity methods

The conductivity (or resistivity) of concrete has been studied and shown that concrete could be viewed as an electrolyte that might conduct electrical current by the movement of the ion in the evaporated liquid through the pore network of the paste matrix (Monfore 1968). The utilization of the concept of the concrete electrical resistivity in structural health monitoring had been further reviewed by Chung (2003). Recently, Andrade et al. (2009) has proposed the use of electrical resistivity as NDT method for the specification of the durability of reinforced concrete. Meanwhile, Wiwattanachang and Giao (2011) used electrical resistivity imaging technique to monitor the crack development in fiber concrete beam.

Lataste et al (2003) presented a crack measurement and monitoring method by evaluating the electrical resistivity of the concrete structures. A four-probe square arrayed device was designed in which two adjacent probes acted as current injection electrodes while the other two acted as measuring electrodes for potential difference measurement. Figure 2.4 illustrates the equipments which are needed to perform the crack measurement by examining the electrical resistivity of the concrete structure. A known electrical intensity was injected into the concrete and the potential difference created by the passage of the current in the concrete was measured. The electrical resistivity was then deducted to assess the depth and width of the crack. This measurement concept was recognized to be a useful method for crack characterization in structural health monitoring (Shah and Ribakov, 2008). Boulay et al. (2009) had proven the sensitivity of the method by showing that the conductance (reciprocal of resistivity) is instantaneously proportional to the mean crack width on

the concrete surface. However, in Boulay's work, the study of the crack widths measurement was limited within the range of 100  $\mu\text{m}$  and the resolution of the method is not mentioned. For practical on-site usage, more studies are needed to eliminate the disturbance factors of moisture condition and salt content (Lataste et al, 2003).

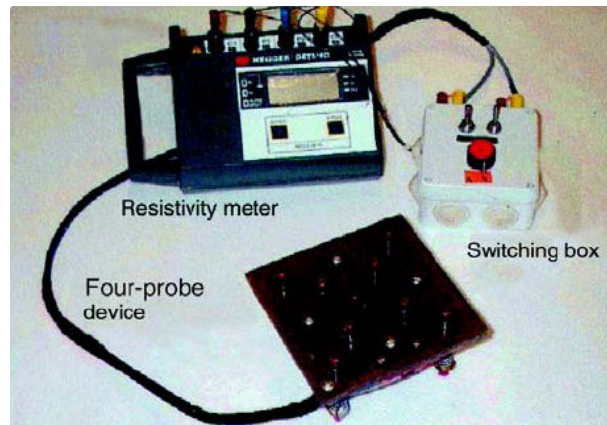


Figure 2.4: Equipments for electrical resistivity measurement on concrete structures.

(Source: Lataste et al., 2003)

A potential application of the resistivity method for crack measurement and monitoring was presented by Lataste et al. (2003) and Boulay et al. (2009). The sensitivity and the response to the change of the crack were also shown. One should be aware that the application of this method depends on the electrolytic behavior of the concrete paste. In practice, the ambient temperature and weather could further dry or moisten the concrete structures. Both types of weathering effects could affect the performance of the method. This method, in fact, measures the potential difference between the two points by the measuring probes. Thus, it could only be considered as a 1-D crack measurement device. No information will be available on the mode II crack (sliding mode). Since electrical charge must be injected into

concrete structures to measure the crack, concern on the safety issue long term monitoring of the crack growth remains doubtful. Further study and development should be carried out to improve the method.

### **2.3.5 Fiber optic sensor (FOS)**

The application of the fiber optics sensor (FOS) is based on the concept that the optical fiber would experience geometrical (size and shape) and optical (refractive index and mode conversion) changes due to various environmental perturbations e.g. temperature and strain. Such changes could affect the optical properties of the transmitted light in terms of amplitude (intensity), phase, frequency, wavelength and polarization. The difference between the transmitted light and the source can be detected and translated into displacement by appropriate interrogation systems (Li et al., 2004a).

FOS has been utilized in structural health monitoring since 1980s. The monitored targets include buildings or edifices, piles, highways, railways, bridges, pipelines, tunnels and dams. In structural health monitoring, the FOSs are utilized for various monitoring application including surface cracks and internal cracks measurement and monitoring, strain in concrete structures as well as the temperature variation (Bassam et al. (2011), Dai et al. (2009), Zhang and Wu (2008), Childs et al. (2008), Chung and Kang (2008), Wan and Leung et al. (2007a), Zhang and Ansari (2005), Li et al. (2004b), Glišić and Inaudi (2002)). The study and development of the FOS for surface cracks monitoring remains an active area as the FOS has the potential to replace the traditional electrical sensors (e.g. LVDT and strain gauge)

with lower cost and higher performance (Li et al., 2004a). A thorough review of the recent application of FOS in SHM has been carried out by Li et al. (2004a) and particularly, the application of Fiber Bragg Grating (FBG) FOS in structural health monitoring was presented by Majumder et al. (2008).

The relationship between the surface crack opening displacement (crack width) and the properties of transmitted light in FOSs was also studied. Leung et al (2007, 2007, 2005 and 2000) researched the application of the FOS in surface cracks measurement and monitoring by relating the optical power loss and the crack width. The magnitude of the power loss was directly proportional to the crack openings. In the study, the proposed FOS scheme was able to detect the crack openings of about 0.1 mm (Leung et al., 2000). Wan and Leung (2007b) further presented a “zigzag” arrangement of a pair of FOSs with opposite angle to detect mix-mode cracks (mode I and II cracks) in concrete structures (Figure 2.5). Ansari et al. (2007, 2006, 2005 and 1996) studied the correlation of the strain of the optical fiber due to the crack opening displacement and the light intensity variation of speckle pattern due to mode redistribution in a multimode fiber. The demonstration showed high linearity in the correlation relationship between two parameters with zero intercept, 1.37% error rate and 95.42% confidence level (Zhang and Ansari, 2006).



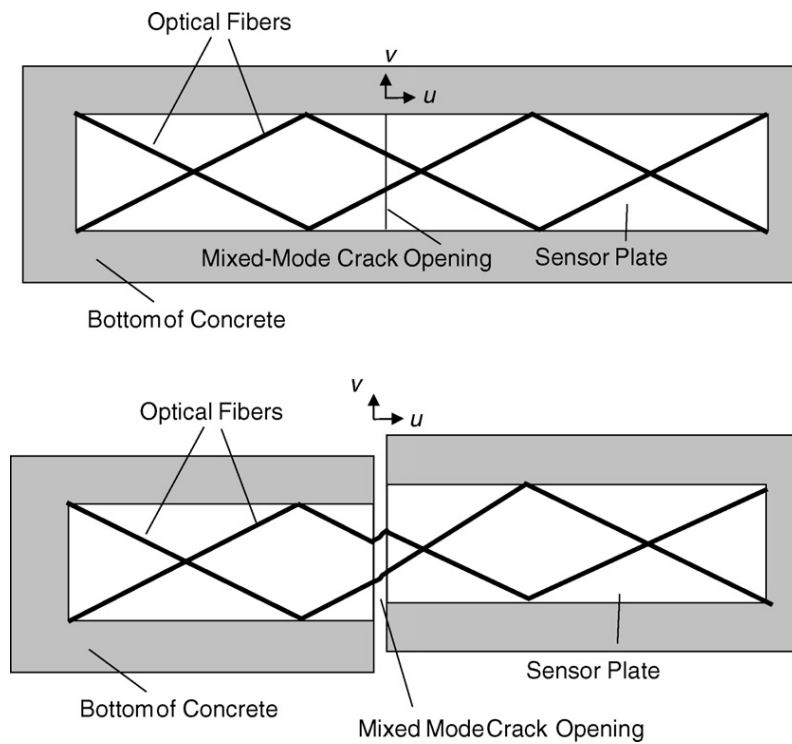


Figure 2.5: (a) Mixed mode crack sensor with two optical fibers at opposite angles and (b) the expected deformation of the optical fiber across crack under mixed mode crack opening. (Source: Wan and Leung, 2007b)

Solid data on the sensitivity of using FOS in crack monitoring is still not available. Leung et al. (2005) had suggested that the sensitivity of the FOS depends on the type of optical fiber and the angle of intersection of the fiber with the cracks direction. Further study is still needed so that the application of the FOS in cracks monitoring could achieve higher accuracy and reliability. However, in the works by Leung et al. (2007) and Ansari et al. (2006), good agreement was achieved between the experimental data (LVDT readings) and the FOS measured data.

The embedment of the optical fiber in the concrete structures needs serious considerations. The optical fiber should be fixed firmly and without having the risk